Progress in Additive Manufacturing
https://doi.org/10.1007/s40964-020-00121-x

FULL RESEARCH ARTICLE

Laser powder bed fusion of 30CrNiMo8 steel for quenching and tempering: examination of the processability and mechanical properties

Livia Zumofen[1] · **Andreas Kirchheim**[1] · **Hans-Jörg Dennig**[1]

Received: 31 January 2020 / Accepted: 11 February 2020

Abstract

The layer-by-layer principle of additive manufacturing technology laser powder bed fusion (LPBF) opens up completely new possibilities in the design and manufacturing of lightweight and efficient gear components. For example, integration of contour conform cooling and lubrication channels into gear components can increase their service life and reduce lubricant consumption. Steels for quenching and tempering and case hardening steels are commonly used materials for gear components. However, the availability of these alloys for LPBF processing is still limited. In particular, the 30CrNiMo8 steel for quenching and tempering is frequently used for gear wheels. This specific alloy is largely unknown regarding LPBF processing and remains challenging, because of its susceptibility to cracking and the high temperature gradients that occur during the LPBF process. Therefore, this study focuses on the LPBF processing of 30CrNiMo8 powder material including process parameter evaluation and material characterization. Additionally, effects of the heat treatment on the resulting microstructure and mechanical properties were investigated. Within this study the 30CrNiMo8 has been processed successfully with a density of well above 99.5% leading to promising mechanical properties. A more homogenous microstructure has been achieved with quenching and tempering, compared to the as-build state.

Keywords Additive manufacturing · Laser powder bed fusion · Laser beam melting · Steel for quenching and tempering · 30CrNiMo8 (AISI 4340) · Mechanical properties

1 Introduction

Additive manufacturing (AM) includes many emerging technologies that allow the layer-wise generation of complex structures based on three-dimensional models. AM is finding more and more applications in numerous sectors, such as medical technology, aerospace, automotive and mechanical engineering industry, leading to its enormous upward trend [1]. Laser Powder Bed Fusion (LPBF) is one of the most common AM processes for metals. Thereby, metal powder is melted selectively with a laser beam to generate complex metal structures, layer by layer. Within the past years, many iron-based alloys with low carbon contents were successfully processed with LPBF, resulting in high-quality parts with comparable mechanical properties to bulk materials [2, 3]. In combination with the enormous design freedom enabled by LPBF, this opens up completely new possibilities in the design and manufacturing of gear components, such as gear wheels. Integration of contour conform cooling and lubrication channels have the potential to increase their service life and reduce lubricant consumption. Through lightweight construction using topology optimization, the moments of inertia of gear wheels can be reduced, which may lead to a higher efficiency and better running properties [4–7].

Steels for quenching and tempering and case hardening steels are commonly used materials for gear components. However, the availability of these alloys for LPBF processing is still limited. The rapid cooling rates and high process-related temperature gradients promote the formation of martensite, which in turn increases the susceptibility to cracking of these materials [8]. Particularly the carbon content, but also other alloying elements affect the weldability of steels [8, 9]. Parameter studies with the high-speed steel

✉ Livia Zumofen
livia.zumofen@zhaw.ch

[1] Centre for Product and Process Development, School of Engineering, Zurich University of Applied Sciences, Winterthur, Switzerland

Published online: 20 February 2020

M2 showed that even relative densities of above 99% are possible with a high carbon content of above 0.8%, although the challenge of internal stresses remained [10, 11]. The literature reports on the following case-hardening steels to be available in powder form and being processed with LPBF: 21NiCrMo2, 15NiCrMo13, 20MnCr5 and 16MnCr5 [4, 6, 7, 12]. The processability of case hardening steel 16MnCr5 has been studied in detail with the intention to build gear wheels in LPBF [6, 7]. Recently, LPBF processing of the steel for quenching and tempering 42CrMo4 (AISI 4140) led to a high part quality with low porosity, no cracking and promising mechanical properties with optimum process parameters [13, 14]. In particular, the 30CrNiMo8 steel for quenching and tempering is frequently used for gear wheels and other transmission components. In early studies, crack formation when processed with LPBF was explained with the chemical composition, fast cooling rates and the remaining oxygen in the build chamber [15]. However, quenched and tempered steel 30CrNiMo8 is still largely unknown in additive manufacturing, especially regarding the processing with lasers operated in pulsed mode.

Therefore, the following examination focuses on the processability, effects of parameters on porosity and cracking and resulting mechanical properties of quenched and tempered steel 30CrNiMo8 with LPBF. The cracking issues are addressed by the use of a baseplate heating system. Furthermore, the effect of heat treatment on microstructure and mechanical properties will be studied. These results will represent the basis for the manufacturing and testing of gear wheels in and to further advance AM of transmission components.

2 30CrNiMo8 powder material

Gas atomized steel for quenching and tempering 30CrNiMo8 powder with a chemical composition lying in the range specified for this material in the DIN EN 10083 norm (Table 1) was used for all experiments. Scanning electron microscopy (SEM) revealed the uniform spherical shape of the powder particles and the presence of a few satellites (Fig. 1a). No pores were found on metallographic cross-sections of powder particles (Fig. 1b). The particle size distribution was 28.8 µm (D_{10})–59.7 µm (D_{90}) featuring a Gauss distribution, measured with a CILAS 1064 particle size analyzer based on the principle of laser diffraction.

3 Methods and experimental setup

3.1 Parameter study

For the present contribution, a Renishaw AM400 HT laser melting system was used, which was equipped with a 400 W SPI fiber laser operated in pulsed mode with a spot size of 70 µm. Unlike continuous lasers, in pulsed mode two distinctive parameters, the point distance and the exposure time, are deployed to define the scan velocity. The point distance corresponds to the distance of each exposure point of the laser, whereas the exposure time defines the duration of the laser exposure. The AM400 was retrofitted with a high temperature (HT) baseplate heating system, which was used to heat the baseplate up to 300 °C for all experiments. A carbon brush was used for recoating, due to the high preheating temperature and to avoid process interruptions. To create

Table 1 Chemical compositions of 30CrNiMo8 in percent per mass according to a DIN EN 10083 and b powder supplier certificate

	C	Si	Mo	Mn	Cr	Ni	Fe
a	0.26–0.34	< 0.4	0.3–0.5	0.3–0.6	1.8–2.2	1.8–2.2	Res
b	0.3	0.28	0.42	0.45	2.0	2.1	Res

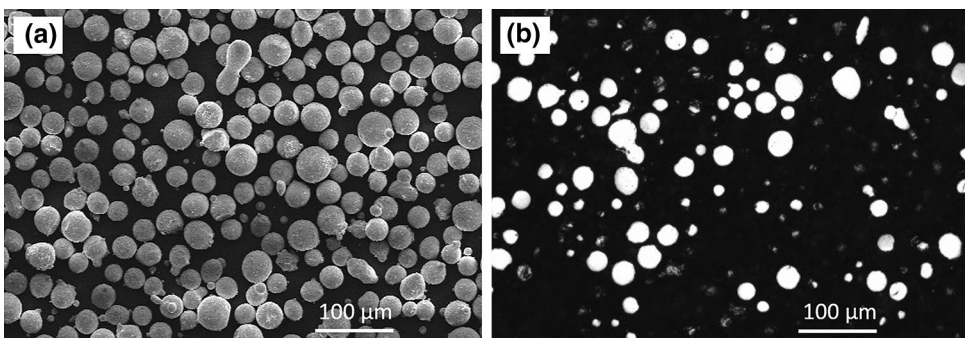

Fig. 1 SEM image (**a**) and cross-section (**b**) of 30CrNiMo8 powder

an inert atmosphere and minimize oxidation during the laser melting process argon gas was used as process gas.

An essential quality criterion when qualifying new materials for LPBF are porosity and lack of fusion, which directly affects the resulting mechanical properties [3, 16]. The formation of imperfections such as porosity, lack of fusion or cracks is strongly connected to the applied process parameters and prevalent process condition [16–18]. Therefore, the specific process parameters need to be combined in a way that allows the formation of a homogenous and stable melt track to minimize imperfections. An adequate energy input assures that each powder layer is fully melted and connected to the underlying material.

To evaluate the effect of the energy density but also different parameter combinations on the relative part density, a full factorial experiment based on the parameters laser power and the exposure time was carried out (Fig. 2). According to Eq. (1) [19] the energy density related to each parameter combination was determined based on the laser power (P_L), scan velocity (v_S), hatch space (s_H) and layer thickness (t_L). The scan velocity was determined from the point distance (s_P) and the exposure time (t_E) (2). Although the energy density is an effective way of comparing various parameter combinations, there is still a variation of part density with constant energy density [20]. This indicates, that the individual parameters have a different effect on meltpool formation and wetability of the melt and thus on the process stability.

$$E_D = \frac{P_L}{v_S \cdot s_H \cdot t_L} \tag{1}$$

$$v_S = \frac{s_P}{t_E} \tag{2}$$

The hatch spacing of 80 µm, point distance of 50 µm and layer thickness of 40 µm were set constant, whereas laser power and exposure time were varied between 160–260 W and 40–80 µs respectively resulting in energy densities between 40 and 130 J/mm^3 (Fig. 2). For each possible combination of these parameters, cubes of $5 \times 5 \times 10$ mm^3 were built with a rotating scan pattern and a rotation angle of 67° between each layer. The cubes were cut in half (horizontally) to examine the porosity and imperfections with metallographic cross-sectioning (Fig. 2).

3.2 Material characterization

Based on the parameter study, further material characterization was carried out with the most economic parameter combination, thus allowing for a high build rate and minimum porosity (see chapter 4), which was applicable at 220 W laser power and 60 µs exposure time. For the upscaling, a checkerboard scan pattern with 5 mm field size was applied. Therefore, three larger cubes of $15 \times 15 \times 15$ mm^3 were built and sanded on all sides to analyze the Archimedes density according to DIN EN ISO 3369 using a KERN ABJ 220-4NM precision balance and distilled water as displacement fluid. To assess the mechanical properties of 30CrNiMo8 processed with LPBF depending on the build orientation, cylindric and cuboid blanks for tensile and notch impact testing were built horizontally and vertically. For each state 3 specimens were built. Tensile specimens were machined according to DIN 50 125 to create B5 × 25 tensile specimens and tested according to EN ISO 6892-1. Notch impact specimens were honed, V-notched and tested according to DIN EN ISO 148-1. Half of the blanks were heat-treated before machining. The heat treatment included the hardening at 850 °C, quenching in oil and tempering at 560 °C. The results were statistically evaluated using the two-tailed *t* test. Results were considered significant with a probability level of $p < 0.01$.

Exposure time [µs] \ Laser power [W]	160	180	200	220	240	260
40	*40*	*45*	*50*	*55*	*60*	*65*
50	*50*	*56*	*63*	*69*	*75*	*81*
60	*60*	*68*	*75*	*83*	*90*	*98*
70	*70*	*79*	*88*	*96*	*105*	*114*
80	*80*	*90*	*100*	*110*	*120*	*130*

Energy density (E_D) [J/mm³]

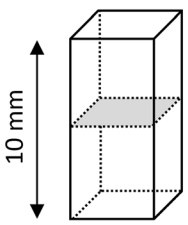

Fig. 2 Full factorial parameter study with laser power and exposure time and corresponding energy densities. For each parameter combination $5 \times 5 \times 10$ mm^3 cubes were built, cut in half (horizontal) and polished to investigate porosity

4 Results and discussion

The part density was strongly affected by the corresponding energy density and parameter combination (Fig. 3). The minimum energy density of 40 J/mm^3 at 160 W laser power and 40 µs exposure time led to the highest porosity within the investigated range. Large spherical pores but also irregularly shaped imperfections were observed on the metallographic cross-section. In general, increasing exposure time led to decreasing porosity on each of the evaluated laser power settings. With increasing exposure time, the relative scan velocity decreased accordingly with the point distance remaining constant. Therefore, porosity decreased with increasing energy density up until the minimum required energy density to form a homogenous melt track is exceeded. Specimens with exposure time ≥ 60 µs and energy density above 75–80 J/mm^3 primarily showed very few small spherical pores (Fig. 3, dotted line), presumably gas pores. Furthermore, no cracks were found on these specimens. The 30CrNiMo8 has a relatively high content of the alloying elements Cr, Ni and Mo, decreasing the critical cooling rate and increasing the ductility of the alloy [8, 21]. This, in combination with preheating to 300 °C, might explain the absence of cracking when processed with LPBF and a suitable parameter combination. Although various parameter combinations and a broad range of energy density led to a low porosity, a low porosity was not guaranteed for a specific energy density level. For example, the two samples at 75 J/mm^3 revealed a distinctively differing porosity, whereas the two samples with 90 J/mm^3 showed similar results. This finding correlates to the findings of Gu et al. and Schmitt et al. [12, 20], suggesting, that not only the energy density but also a suitable combination of the specific parameters is crucial for a high part quality.

To allow for an economic process with a rapid build rate and minimum porosity, the parameter combination of 220 W laser power and 60 µs exposure time was chosen for further material characterization. Archimedean density measurement led to a relative density of 99.76% ± 0.07% for this specific set of parameters.

Optical micrographs of a vertical cross-section revealed longitudinally elongated grains in build direction in the as-built state (Fig. 4a). Additionally, the layer-wise buildup of the material can be recognized in the form of horizontally aligned slightly brighter and darker stripes in the microstructure. With quenching and tempering, a fine acicular microstructure is formed, as it is typical for 30CrNiMo8 alloy (Fig. 4b). Overall, a more homogenous microstructure was present after quenching and tempering, with no evident orientation related texture. Compared to the quenched and

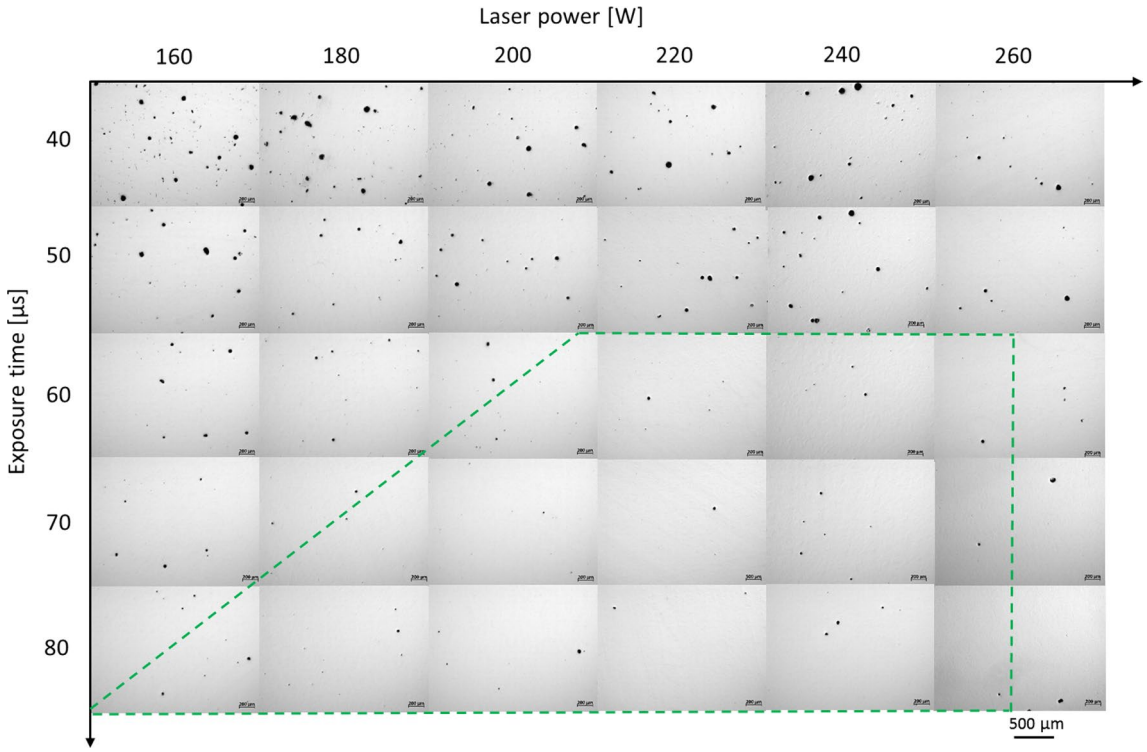

Fig. 3 Metallographic cross-sections (horizontal) of cubes built in a parameter study with varying laser power (160–260 W) and exposure time (40–80 µs). The dotted line surrounds the area with the lowest porosity

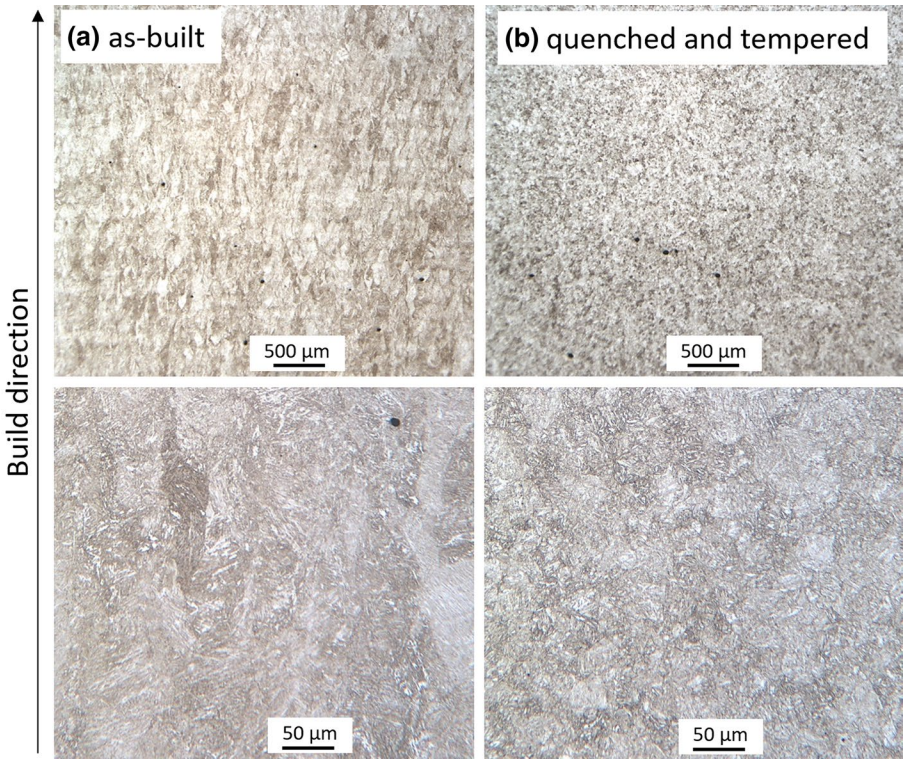

Fig. 4 Optical micrographs of a vertical cross-section in the as-built (**a**) and quenched and tempered (**b**) state, etched with 3% Nital

tempered state, as-built material showed a coarser acicular microstructure. This might be accounted to the inevitable reheating of the material with each new layer and the slower cooling rates compared to the current layer, leading to a tempering alike heat treatment during the LPBF process.

Tensile and notch impact tests showed promising mechanical properties of 30CrNiMo8 processed with LPBF (Fig. 5). Yield strength and tensile strength of quenched and tempered specimens were 1009–1016 MPa and 1094–1098 MPa respectively, which is comparable with bulk material with a similar heat treatment [22]. Also, the elongation at break of 14.2–16.9% (quenched and tempered) goes in line with literature values [22]. Notch impact tests revealed remarkably high impact energies of 99–109 J for LPBF processed 30CrNiMo8 in the quenched and tempered state compared to bulk material [21], indicating high ductility.

It is expected, that this is a result of the unique microstructure formed during LPBF and subsequent quenching and tempering. To allow a comprehensive explanation of the interplay between the processes involved, further investigations are needed.

In the as-built state, the yield strength was significantly higher for horizontally oriented specimens compared to the vertical orientation, $t(2) = -21.6$, $p < 0.001$. This finding is most probably related to the microstructure showing a preferred grain growth in build direction, due to the layer-by-layer principle of LPBF. The connection of lower yield strength in build direction (Fig. 5) and vertically oriented columnar grains (Fig. 4) is a frequently observed phenomenon in LPBF processing of metals [18]. Due to the layer by layer manufacturing, the formation of each new layer leads to a heat transfer into the material below, depending on the distance from the current layer. Thereby, the material undergoes a cyclic change in temperature and varying cooling rates. This is also referred as intrinsic heat treatment and affects the microstructure and mechanical properties of the material [14].

There was a slightly higher variation of the mechanical properties in build direction, which corresponds to the vertical orientation. This might indicate a more heterogenous microstructure in build direction compared to the *XY*-plane (horizontal) for the as-built state. Quenching and tempering led to equalized yield strength and tensile strength of the evaluated orientations, which correlates to the homogenous microstructure observed in optical micrographs (Fig. 4b). Tensile strength was almost as high in the as-built as in the quenched and tempered state, which also might be related to the intrinsic heat treatment during LPBF, which is comparable to tempering after initial rapid cooling. However, the intrinsic heat treatment leads to an inhomogeneous microstructure and orientation related texture as mentioned above. Therefore, the quenching and tempering after LPBF are still recommended to achieve a more homogenous microstructure and mechanical properties.

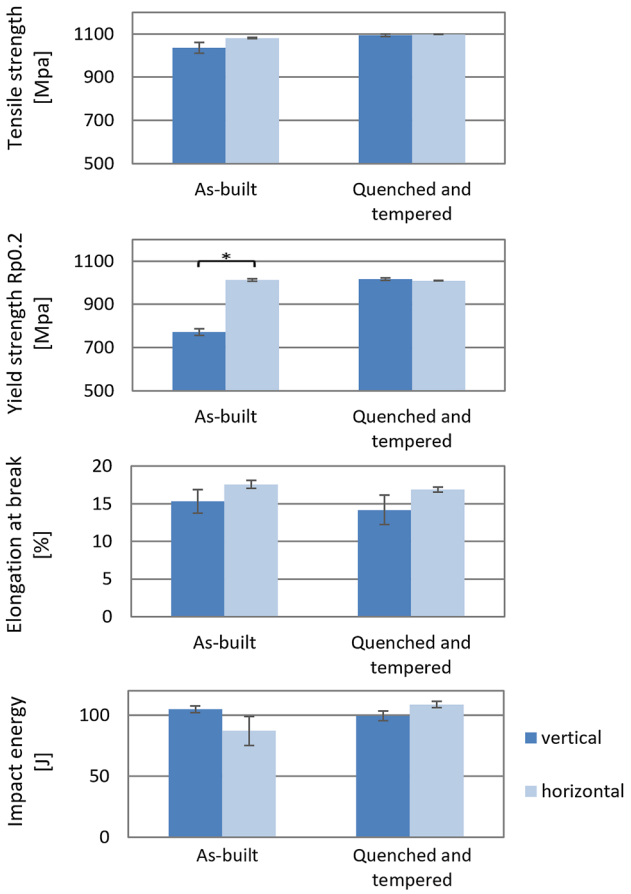

Fig. 5 Tensile properties and impact energy of vertically and horizontally oriented specimens in the as-built and in the quenched and tempered state. Columns and indicators represent mean values ± standard deviations. *Significant result with $t(2) = -21.6$, $p < 0.001$

Fig. 6 Gear wheel demonstrator with internal cooling channels manufactured with LPBF

Based on the set of parameters described in Sect. 3.2, gear wheels with internal cooling channels have been successfully manufactured with LPBF (Fig. 6).

5 Conclusion and further work

Within this study, the processability of steel for quenching and tempering with LPBF has been proven. A parameter study based on the variation of laser power and exposure time led to several parameters with very low porosity. Based on the set of parameters offering a rapid build rate and minimum porosity ($99.76 \pm 0.07\%$), further material characterisation was carried out. Thereby, the effect of heat treatment and the build orientation on microstructure and mechanical properties was investigated. In the as-built state, columnar grains arranged in build direction were present. Quenching and tempering led to a more homogenous microstructure with no evident orientation related texture. Tensile properties after quenching and tempering were comparable to the bulk material. Notch impact testing led to very high impact energies, indicating a high ductility of the material. In summary, very promising mechanical properties were achieved, particularly for the quenched and tempered state. Further work will focus more closely on the formation of the microstructure, the fracture behaviour, the potential presence of microcracks and the effects of the intrinsic heat treatment. Furthermore, these results represent the basis for the manufacturing of gear wheels with internal cooling channels, which will be tested on a specifically developed test bench.

Acknowledgements We extend our sincere thanks to the Swiss Innovation Agency (Innosuisse) and the industry partner RENK-MAAG GmbH for funding and supporting this research within the research Grant 25648.1 PFIW-IW. The authors also thank Mr. Tobias Fritsche and Mr. Yogeshkumar Katrodiya for their assistance.

References

1. Wohlers T, Caffrey T (2018) Wohlers report 2018. 3D-printing and additive manufacturing state of the industry—annual worldwide progress report. Wohlers Associates, Fort Collins
2. Bourell D, Kruth JP, Leu M, Levy G, Rosen DW, Beese AM, Clare A (2017) Materials for additive manufacturing. CIRP Ann Manuf Technol 66:659–681. https://doi.org/10.1016/j.cirp.2017.05.009

3. Yap CY, Chua CK, Dong ZL, Liu ZH, Zhang DQ, Loh LE, Sing SL (2015) Review of selective laser melting: materials and applications. Appl Phys Rev 10(1063/1):4935926
4. Rogers K (2019) Additive manufacturing technologies for gears, American Gears Manufacturing Association published by Barners Group Advisors
5. Siglmüller F, Kupfer S, Kamps T, Schmitt M, Lohner T, Reinhart G, Stahl K (2018) Efficiency of additive manufactured gears with conformal cooling. In: 21st TAE International Colloquium Tribology, Stuttgart
6. Kamps T (2018) Leichtbau von Stirnzahnrädern aus Einsatzstahl mittels Laserstrahlschmelzen, Dissertation, Technische Universität München
7. Schmitt M, Jansen D, Bihlmeir A, Anstätt JC, Schlick G, Tobie T, Stahl K, Reinhart G (2019) Rahmen und Strategien für den Leichtbau von additiv gefertigten Zahnrädern für die Automobilindustrie. Rapid.Tech—Fachkongress, Erfurt
8. Fahrenwaldt HJ, Schuler V (2011) Praxiswissen Schweißtechnik. Vieweg+Teubner Verlag, Springer Fachmedien, Wiesbaden
9. Matthes KJ, Schneider W (2016) Schweisstechnik. Fachbuchverlag Leipzig im Carl Hansen Verlag, München
10. Kempen K, Thijs L, Vrancken B, Buls S, Van Humbeeck J, Kruth JP (2013) Producing crack-free, high density M2 Hss parts by selective laser melting: pre-heating the baseplate. In: Proceedings 24th International Solid Freeform Fabrication Symposium, pp 131–139
11. Zumofen L, Beck C, Kirchheim A, Dennig HJ (2017) Quality related effects of the preheating, temperature on laser melted high carbon content steels. In: Proceedings of additive manufacturing in products and applications—AMPA2017, Springer. https://doi.org/10.1007/978-3-319-66866-6_21
12. Schmitt M, Schlick G, Seidel C, Reinhart G (2018) Examination of the processability of 16MnCr5 by means of laser powder bed fusion. In: 10th CIRP conference on photonic technologies
13. Wang W, Kelly S (2016) A metallurgical evaluation of the powder-bed laser additive manufactured 4140 steel material. Miner Metals Mater Soc 68(3). https://doi.org/10.1007/s11837-015-1804-y
14. Damon J, Koch R, Kaiser D, Graf G, Dietrich S, Schulze V (2019) Process development and impact of intrinsic heat treatment on the mechanical performance of selective laser melted AISI 4140. Addit Manuf 28(2019):275–284. https://doi.org/10.1016/j.addma.2019.05.012
15. Jelis E, Clemente M, Kerwiens RNM, Hespos MR (2015) Metallurgical and mechanical evaluation of 4340 steel produced by direct metal laser sintering. JOM 67(3):582–589
16. Liverani E, Toschi S, Ceschini L, Fortunato A (2017) Effect of selective laser melting (SLM) process parameters on microstructure and mechanical properties of 316L austenitic stainless steel. J Mater Process Technol 249:255–263. https://doi.org/10.1016/j.jmatprotec.2017.05.042
17. Kruth JP, Froyen L, Van Vaerenbergh J, Mercelis P, Rombouts M, Lauwers B (2004) Selective laser melting of iron-based powder. J Mater Process Technol
18. Herzog D, Seyda V, Wycisk E, Emmelmann C (2016) Additive manufacturing of metals. Acta Mater 117:371–392. https://doi.org/10.1016/j.actamat.2016.07.019
19. Thijs L, Verhaeghe F, Craeghs T, Van Humbeeck J, Kruth JP (2016) A study of the microstructural evolution during selective laser melting of Ti-6Al-4V. Acta Materialia Inc. Published by Elsevier Ltd. https://doi.org/10.1016/j.actamat.2010.02.004
20. Gu H, Gong H, Pal D, Rafi K, Starr T, Stucker B (2013) Influences of energy density on porosity and microstructure of selective laser melted 17-4PH stainless steel. In: Solid freeform fabrication symposium
21. DIN EN 10083-3 (2017) Steels for quenching and tempering - Part 3: Technical delivery conditions for alloy steels, English version, of DIN EN 10083-3: 2017-01, Deutsches Institut für Normung e. V., Berlin
22. Warlimont H, Martienssen W (eds) (2018) Springer handbook of materials data, 2nd edn. Springer Nature https://doi.org/10.1007/978-3-319-69743-7